CONSILIENCE IN DISEASE ECOLOGY: FMDV TRANSMISSION DYNAMICS REFLECT VIRAL GROWTH AND IMMUNE RESPONSE RATES. *

J. C. Macdonald[a,b,], **H. Gulbudak**[a,1], **B. Beechler**[c], **E. Gorsich**[d], **S. Gubbins**[e], **E. Perez-Martin**[e], **A. Jolles**[c,f,1]

[a] Department of Mathematics, University of Louisiana at Lafayette, Lafayette, Louisiana, USA [b] Current address, School of Zoology, Faculty of Life Sciences, Tel Aviv University, Tel Aviv-Yafo, Israel [c] Carlson College of Veterinary Medicine, Oregon State University, Corvallis, Oregon, USA [d] The Zeeman Institute for Systems Biology Infectious Disease Epidemiology Research and School of Life Sciences, The University of Warwick, Coventry, UK [e] The Pirbright Institute, Woking, Surrey, UK [f] Department of Integrative Biology, Oregon State University, Corvallis, Oregon, USA [1] The authors for correspondence, HG: hayriye.gulbudak@louisiana.edu, AJ: aejolles@gmail.com

ABSTRACT

Infectious disease dynamics operate across biological scales: pathogens replicate within hosts, but transmit among hosts and populations. Functional changes in the pathogen-host interaction thus generate cascading effects from molecular to landscape scales. We investigated within-host dynamics and among-host transmission of three strains of foot-and-mouth disease viruses (FMDVs) in their wildlife host, African buffalo. We combined data on viral dynamics and host immune responses with mathematical models to ask (i) How do viral and immune dynamics vary among FMDV strains? (SAT1, 2, 3); (ii) Which viral and immune parameters determine viral fitness within hosts?; and (iii) How do within-host dynamics relate to virus transmission among hosts? Our data reveal contrasting within-host dynamics among viral strains. However, SAT2 elicited more rapid and effective immune responses than SAT1 and SAT3. Within-host viral fitness was overwhelmingly determined by variation among hosts in immune response activation rates against FMDVs, but not by variation among individual hosts in viral growth rate. By contrast, our analyses investigating across-scale linkages indicate that viral replication rate in the host correlates with transmission rates among buffalo; and that adaptive immune activation rate determines the infectious period. Together, these parameters define the basic reproductive number, $\mathcal{R}_0$, of the virus, suggesting that viral invasion potential may be predictable from within-host dynamics. Future work should test the generality of these findings by including additional FMDV strains, and create a multi-scale model to link within-host and between-host dynamics explicitly.

***K*eywords** FMDV · Life history · Immune dynamics · Viral dynamics · Route of infection

1 Introduction

Linking pathogen dynamics across biological scales,from cellular and molecular interactions within the host's tissues to transmission among individuals and populations, is critical to understanding ecological and evolutionary trajectories of host-pathogen systems, and represents a central challenge in disease ecology [1–3]. Multi-scale models of infectious disease dynamics seek to address this challenge by linking mechanistic models representing pathogen-host interactions at cellular to population scales. Developing the mathematical tools for connecting dynamic processes operating at vastly different temporal and spatial scales has been an active focus in infectious disease modeling [4–12]; however, these theoretical innovations have so far not been matched by empirical data generation, providing integrated data sets that document infection processes in the same host- pathogen system consistently across organizational scales.

* *Citation*: **Authors. Title. Pages.... DOI:000000/11111.**

In this study, we leveraged experimental data on within-host dynamics, and among-host transmission of three strains of foot-and-mouth disease viruses (FMDVs) in their wild reservoir host, African buffalo (*Syncerus caffer*). We constructed a data-driven mathematical model to understand the interplay between viral population growth and its limitation by the host's immune responses. We then investigated to what extent parameters capturing within-host viral dynamics can predict variation in viral fitness at within- and among-host scales. Within the host we define fitness as viral production in terms of both peak and cumulative viral load. As such these are both measures of relative success. At the population scale fitness is assessed in terms of the basic reproductive number $\mathcal{R}_0$, defined as the mean number of secondary infections caused by a single infected host in a wholly susceptible population. $\mathcal{R}_0$ represents the pathogen's ability to invade susceptible host populations [13]. Thus, our approach connects within-host viral dynamics to the potential for pathogen spread in host populations, providing a first step towards integrating data and disease dynamic models across biological scales in this study system.

FMDVs in African buffalo provide a tractable model system for the study of multi-scale infection processes in natural populations. FMDVs are highly contagious viruses that cause clinical disease and substantial production losses in domestic ungulates, while endemic infections in their wildlife reservoir tend to be milder [14, 15]. FMDVs are ubiquitous in African buffalo [14], with three distinct serotypes circulating in wild buffalo populations essentially independently in Southern Africa [16–18], allowing meaningful comparisons across sympatric viral strains. FMD is the most important trade-restricting livestock disease globally, and as a result, well-established methods exist for virus culture, experimental challenges, diagnostics, and quantifying immune responses [17, 19–22]. Previous work has shown that FMDV strains vary substantially in their transmission dynamics among buffalo hosts [19]; and viral proliferation and immune response patterns in buffalo have been described [23]. However, the functional interplay of within-host viral and immune dynamics has not been evaluated in buffalo, compared among Southern African Territories (SAT) serotypes, or aligned with population-level disease dynamics. In this study, we combined experimental infection data and a mechanistic mathematical model to ask: (i) How do viral and immune dynamic interactions vary among FMDV strains?; (ii) Which viral and immune parameters determine viral fitness within hosts?; and (iii) How do within-host dynamics relate to virus transmission among hosts? Our data and models show that variation among viral strains in dynamics within buffalo hosts is reflected in variation in transmission dynamics among hosts, demonstrating agreement in viral dynamics across biological scales.

2 Results

We conducted transmission experiments in which time series data were collected, both to quantify viral and immune kinetics within each host and to estimate epidemiological parameters such as transmission rate and infectious period for one strain of each serotype for primary (acute) FMDV infection.

To elucidate the interactions between viral and immune kinetics, we consider a model linking within-host viral and immune dynamics [Fig. 1, (1)], which we then fit to three time series for each host: viral load, innate immune response, and adaptive immune response.We assume that the innate response clears pathogen at rate θ. The adaptive immune response, mediated by neutralizing antibodies produced by the host's B cells, clears pathogen at rate δ. Upon virus introduction, the adaptive immune response is activated via two pathways: It ramps up with a rate b independent of the innate response, and responds to alarm signals induced by innate immune activation with a rate $aI(\tau)/(1+I(\tau))$ [24]. Our model includes the pathogen population $[P(\tau)]$, and innate $[I(\tau)]$ and adaptive $[A(\tau)]$ immune effectors, where τ refers to time since infection of the host, and initial conditions (densities) $I(0) = I_0, P(0) = P_0, A(0) = A_0$.

$$\begin{cases} \dfrac{dI}{d\tau} = \Lambda + \dfrac{kP(\tau)}{\gamma + P(\tau)} I(\tau) - dI(\tau) \\ \dfrac{dP}{d\tau} = \left[r\left(1 - \dfrac{P(\tau)}{K}\right) - \theta I(\tau) - \delta A(\tau) \right] P(\tau), \\ \dfrac{dA}{d\tau} = \left[a\dfrac{I(\tau)}{1+I(\tau)} + bA(\tau) \right] P(\tau), \end{cases} \tag{1}$$

We assume that the parasite replicates with a logistic growth rate $r(1 - P(\tau)/K)$, with within-host virus carrying capacity in absence of adaptive immune response, K. Innate immune responses, characterized by a marker of inflammation (haptoglobin) were assessed during experimental infection of buffalo with FMDVs, which yielded the most consistent fits compared to other measures of innate immunity that we assessed [see Supp. Material]. Our models assume that innate immune response effectors are always present at a maintenance level Λ/d in absence of virus. Upon exposure to virus, the inducible innate immune response is activated at maximum rate k with half saturation constant, γ, in terms of viral load, and decays at rate d, fixed at mean values inferred in [20].

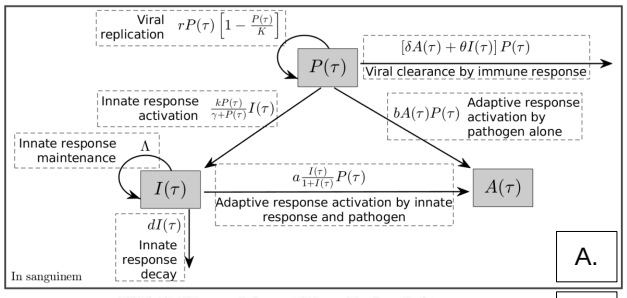

Table 1: Key model quantities with description

Quantity	Description
P_0	Initial viral load allowed range: $[2.1\times10^{-7}, 1]$
r	Viral growth rate allowed range: $[0, 6]$
$\max_\tau P(\tau)$	Maximum viral load, from fit time trajectory
K	Viral carrying capacity *in absence of adaptive response* allowed range: $[3.75, 11]$
$\int_0^\tau P(s)ds$	Cum. viral load at time τ *days*
I_0	Initial innate response level allowed range: $[0.8\mathrm{X}_I^j(0), X_I^j(0)]$ $\log_{10}(\mu g/mL)$ if $X_I^{(j)}(0) > 0$, $[1.5, 2.0]$ $\log_{10}(\mu g/mL)$ if $X_I^{(j)}(0) = 0$
A_0	Initial adaptive response level, fixed at $(1\times10^{-4})I_0$ for fitting
Λ	Innate response maintenance rate, fixed at $d\cdot\min_\tau X_I^{(j)}(\tau)$ for host j
k	Max. innate response activ. rate allowed range: $[0.04, 1]$
γ	Half-saturation constant for innate response activation allowed range: $[0.9P_0^{(j)}, 1.1P_0^{(j)}]$.
d	Decay rate of innate response fixed at $d = 1/11.18$ $days^{-1}$ for SAA, $d = 1/21.23$ $days^{-1}$ for Hapto, from Glidden et al. 2018.
a	Adaptive response activation rate due to innate response, for fitting $a = 0$.
b	Adapt. resp. activ. rate due to path., allowed range: $[0, 1]$
δ	Clearance rate of adaptive response allowed range: $[0, 3]$
θ	Clearance rate of innate response for fitting $\theta = 0$.

Figure 1: (a) Model diagram corresponding to system (1), compartments are pathogen, P, innate immune response, I, adaptive immune response, A. (b) Key model quantities and parameters with description

Our model captures the viral and immune dynamics occurring within individual buffalo hosts, and model parameters are identifiable given the data that we collected [Fig. 2, SI section C]. In particular, we note that across 11 contact infected hosts the mean average relative error is well below the introduced noise level of 40%.

As an additional reality check for our models, we compared model output against data on fevers mounted by the animals. The model-inferred time course of immune and viral dynamics was reasonable in the context of clinical signs [see [23] for details of the temperature data and the shaded boxes in Fig. 2 for visual representation of these inferred fever quantities]. There was some variability among viral strains and individual hosts in the timing and magnitude of the fever response to FMDV infection. However, for the most part, buffalo mounted fevers, as viral loads peaked, and maintained elevated body temperature until most of the virus had been cleared - as one would expect for an acute viral infection [24].

2.1 Viral and immune dynamics vary among FMDV strains

The three viral strains exhibited contrasting dynamics within buffalo hosts. Relative to experiment start SAT1 attains its maximum viral load most rapidly, on average 3.30 days post-contact, while SAT2 and SAT3 took 4.28 and 5.89 days, respectively [SAT1: 2.96-3.59 days; SAT2: 3.80-4.67 days; SAT3: 5.36-6.34 days; Fig. 3c]. Indeed, viral growth rate

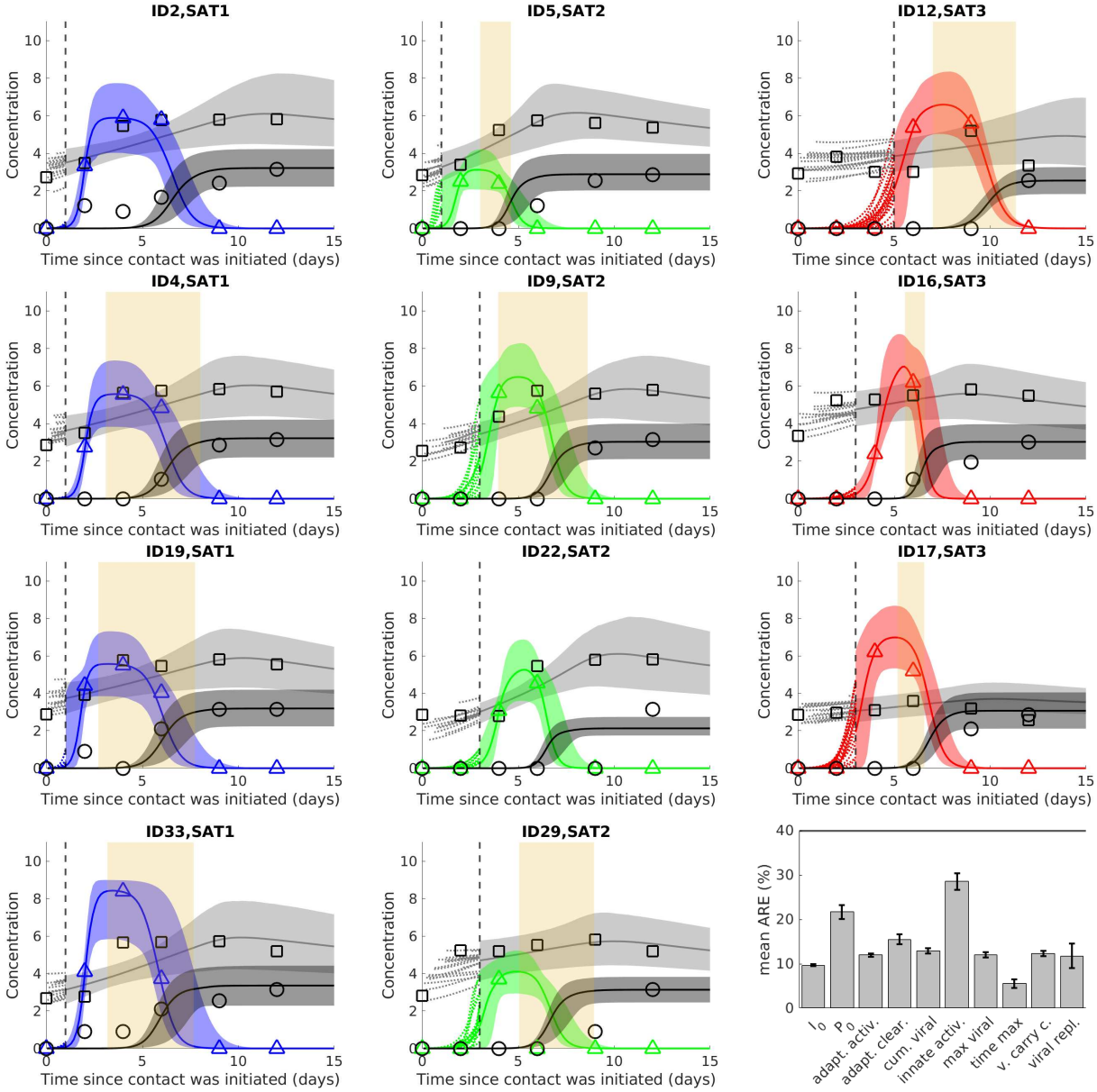

Figure 2: Our model reproduces empirically observed *in vivo* viral and immune dynamics well, and model parameters are identifiable. Vertical dashed line indicates maximum randomly drawn infection start time from [25]. Dotted lines before the maximum start time are a simple random sample of 20 model trajectories from 10,000 generated per host. Median time trajectories (lines) and 95% confidence intervals (shaded regions). Blue indicates SAT1, purple SAT2, red SAT3. Haptoglobin used as measure of innate response (light grey shade) [$\log_{10}(\mu g/mL)$], FMDV viral data (colored shades) [$\log_{10}$(genome copies/mL)], and Virus neutralization titre [$\log_{10}$(VNT)] used as measure of adaptive response (dark grey shade). Yellow shaded region indicates times during which fever was detected. (bottom right) Mean average relative error (ARE) for key model quantities with standard error. Thick black line indicates identifiability threshold corresponding to introduced noise level of 40%. Lack of fever period for host IDs 2, 22 is not indicative of lack of fever, but rather of temperature logger malfunction.

was negatively correlated to both time to maximum viral load, latency period, and infection start time (in contact days) among individual hosts [Fig. 4d,j and Fig. 5a Pearson correlation across median parameter estimates for 11 sample hosts $\varrho = -0.93$, $p = 2.7 \times 10^{-5}$; $\varrho = -0.85$, $p = 8 \times 10^{-4}$; and $\varrho = -0.76$, $p = 0.0043$ respectively]. These relationships point to life history variation among viral strains, where viruses with fast growth rates appear to reach their within-host peak load quickly post initiation of contact.

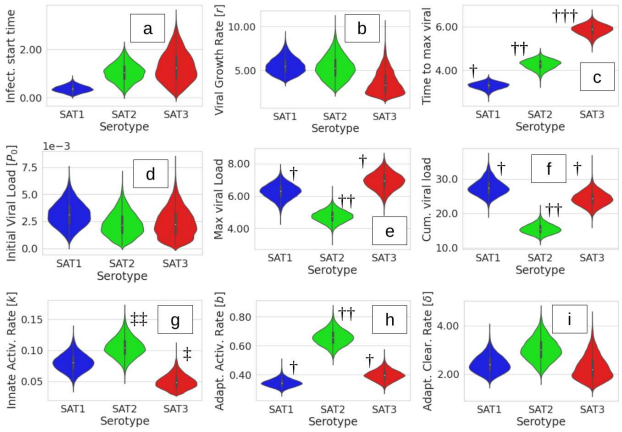

Figure 3: Variation among FMDV serotypes in viral and immune parameters defining within-host dynamics. Violin plots represent serotype sample mean parameters; daggers indicate statistically significant difference

Host immune responses to FMDV infection also varied by strain. Buffalo activated innate immune responses [k] (as measured by haptoglobin, an acute inflammatory protein) more rapidly when infected with SAT2 than SAT3, while SAT1 is intermediate between them [SAT1: 0.081, *CI* 0.0544-0.1100; SAT2: 0.1054, *CI* 0.0754-0.1391; SAT3: 0.0499, *CI* 0.0308-0.0750, Fig. 3g]. I_0 and innate activation rate were negatively correlated among hosts [$\varrho = -0.61$, $p = 0.048$, Fig. 4a], suggesting that individual hosts with low constitutive innate immunity may compensate by quickly ramping up innate responses. Buffalo activated adaptive immune responses, as measured by FMDV neutralizing antibody titer [b], more rapidly for SAT2 than either SAT1 or SAT3 [SAT1: 0.346, *CI* 0.297-0.406; SAT2: 0.658, 0.557-0.767; SAT3: 0.398, 0.329-0.475]. Among individual buffalo, innate and adaptive activation rates were both strongly predictive of viral clearance rate [$\varrho = 0.82$, $p = 0.002$, $\varrho = 0.83$, $p = 0.002$ respectively], indicating variation among hosts in the speed and effectiveness of their immune responses [Figs. 3,4].

2.2 Which viral & immune parameters determine viral fitness within hosts?

The observed differences in viral dynamics and host responses to infection resulted in differences in viral fitness among strains: SAT1 attained high maximum and cumulative viral titers in buffalo hosts. SAT2 lagged conspicuously behind the other two strains in both cumulative and maximum viral load. SAT2's maximum viral load was 76.1% [CI 61.3-93.6%] that of SAT1 and 73.0% [55.9-85.2] of SAT1's and SAT3's respectively; and its cumulative viral load was 56.8% [CI 44.4-71.7 %] lower than the fittest strain (SAT1) [Fig. 3e,f]. Total viral production by each host (cumulative viral load) was driven overwhelmingly by variation among buffalo in adaptive activation rate [Fig. 4f]: a more rapid adaptive immune activation rate (and correlated efficient adaptive clearance [Fig. 4g], was associated with lower cumulative viral load [$\varrho = -0.93$, p = 2.6×10^{-5}]. By contrast, the viral kinetic parameters we assessed (initial viral load, viral growth rate) were not associated with variation in within-host viral fitness directly. These findings suggest that different viral life histories can result in similar fitness in terms of cumulative and maximum viral loads, which is mediated by the viral interaction with the host's immune responses.

2.3 How do within-host dynamics relate to virus transmission among hosts?

To explore how within-host FMDV dynamics might scale up to affect viral transmission among hosts, we compared parameters fit to our within-host model to population-scale parameters derived from the same set of experiments [19]. These analyses indicate that variation in viral growth rate among buffalo correlates tightly and negatively with latent period [Fig. 5a], such that buffalo harboring fast-growing viral populations progress to the infectious class more rapidly. Further, viral growth rate within the host may correlate with variation among viral strains in transmission rates [Fig. 5b]: Fast growing SAT1 transmitted among buffalo most readily, followed by SAT2, while SAT3's slower-paced time to within-host maximum was matched by slower transmission among hosts. Variation among hosts in the rate at which adaptive immune responses against FMDV were activated correlated with each host's infectious period [Fig. 5c].

Together, the transmission rate and infectious period determine the basic reproductive number ($\mathcal{R}_0$) of the virus which can be calculated as $\mathcal{R}_0 =$ (transmission rate)·(infectious period). Our data on cross-scale linkages in viral dynamics suggest that viral invasion potential may be predictable from within-host dynamics. We explored this idea by comparing $\mathcal{R}_0$ established previously [19] by observing transmission of FMDV between hosts, with $\mathcal{R}_0$ calculated based on within

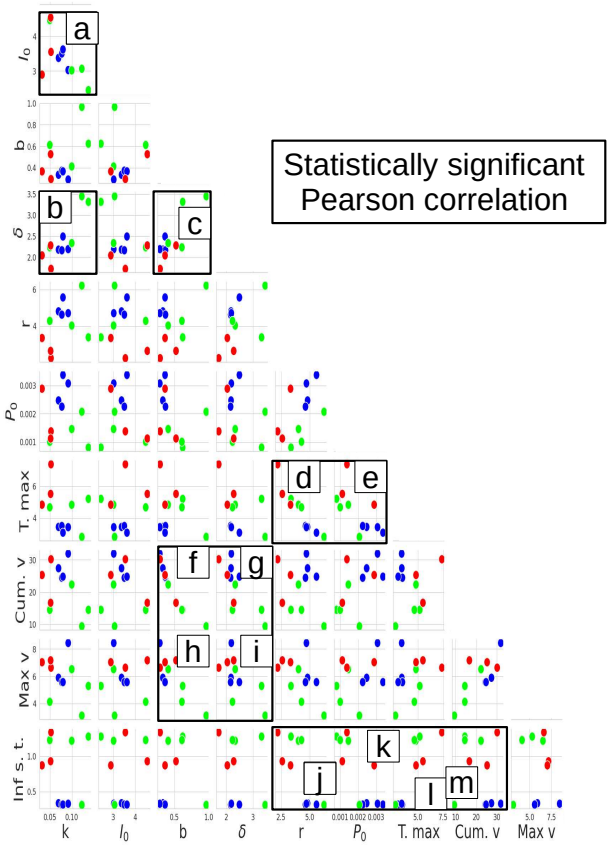

Figure 4: Co-variation between parameters capturing viral and immune dynamics within buffalo hosts. Blue indicates SAT1, green SAT2, red SAT3. Scatter plots show median parameter estimates from 10,000 replications for each host generated by Monte-Carlo simulations. Pairs of parameters that have significant Pearson correlations are framed in solid black lines.

host viral and immune kinetic parameters: We estimated transmission rate and infectious period as linear functions of viral growth rate and adaptive activation rate, respectively, and computed $\mathcal{R}_0$ as their product [see [Fig.5b,c]]. Our data on three strains of FMDV demonstrate a good match between $\mathcal{R}_0$ estimated from within-host parameters with $\mathcal{R}_0$ measured by observing disease transmission among hosts. However, more than three strains of FMDV will need to be studied to test the robustness of this finding. We then compared these basic reproductive numbers derived from within-host viral dynamic parameters [Fig. 5d] to reproductive numbers estimated by observing transmission among hosts in our experiments [19], and found that both estimates of $\mathcal{R}_0$ match qualitatively [Fig. 5d inset].

3 Discussion

In this study, we used time series data from viral challenge experiments involving 11 buffalo acutely infected with three strains of FMDVs (4, 4 and 3 buffalo per strain) to parameterize a mathematical model capturing the dynamics of viral growth and its curtailment by the host's immune responses. We sought to determine: (i) How do viral and immune dynamics vary among FMDV strains?; (ii) Which viral & immune parameters determine viral fitness within hosts?; and (iii) How do within-host dynamics relate to virus transmission among hosts? Despite the moderate number of host individuals included in the study, identifiability analysis of our model parameters suggests that our models capture the data well: Identifability analysis yielded robust interval estimates for model parameters by replicating the sample 10,000 times as well as a metric (average relative error) to assess whether or not model parameters can be reliably identified from available data. Here we found that our model parameters were practically identifiable at an introduced

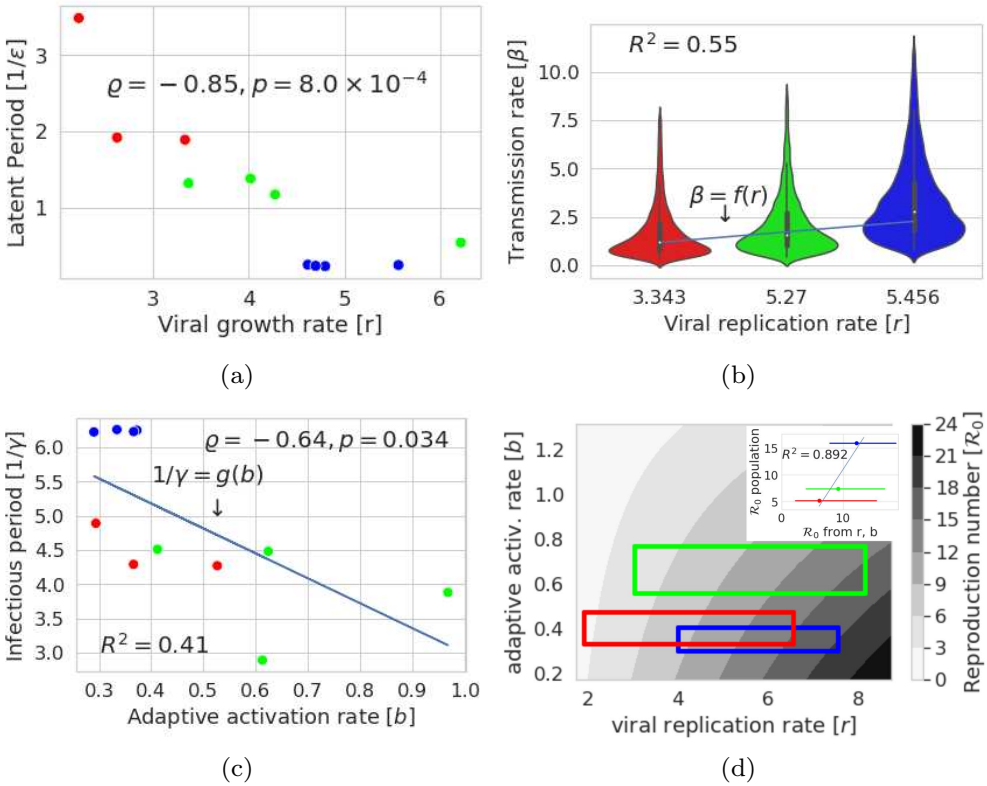

Figure 5: Consilience across scales; (a) Viral growth rate is negatively correlated with latent period (b) sample mean viral growth rate has apparent positive trend with transmission rate (c) adaptive activation rate is negatively correlated with infectious period (d) $\mathcal{R}_0$, a population level quantity which summarizes transmisibility, may be viewed as a function of viral growth rate and adaptive activation rate. Estimate of $\mathcal{R}_0$ obtained from immune scale parameters predicts estimate from population scale model well. Immune parameters (r,b) are from this work and population scale parameters ($1/\gamma$, $1/\epsilon$, β) are from [19]. Points represent median parameter estimates for each contact infected host. Both infectious and latent period were assumed to be gamma distributed, with fit means for latent period: 0.5 *days* [95% CI 0.02-2.4], 1.3 *days* [0.1- 3.5] 2.8 *days* [0.5, 7.0] and shape parameters 1.2 [0.1-8.7], 1.6 [0.2-9.2], 1.6 [0.2-8.3] for SAT1-SAT 3 respectively [19]. Similarly, for infectious period, means were estimated at 5.7 *days* [4.4-7.4], 4.6 *days* [3.5-6.3], and 4.2 days [3.2, 5.8], and shape parameters 11.8 [3.5-33.5], 8.7 [2.4-27.0], 11.8 [3.3-35.3]

noise level of 40% (chosen to cover the original data), and that our results correspond well with independently estimated metrics of fever within the same hosts.

Our results uncover variation among viral strains in within-host dynamics. SAT1 was able to transmit most rapidly, leading to an early peak in viral load, just 3-4 days post start of contact. SAT2 achieved its maximum viral load somewhat more slowly, reaching its peak viral load about a day later than SAT1. By contrast, SAT 3 appeared to follow a strikingly different strategy, attaining its peak viral load a full three days later than SAT1. However, interestingly, despite the large disparity between SAT1 and SAT3 in the time course of viral proliferation within the host, within-host fitness of these strains was quite similar: SAT1 and SAT3 attained similar maximum and cumulative viral loads. By both of these measures, SAT2 had sharply reduced fitness compared to the other two strains - despite kinetic similarities with SAT1. This contrast appeared related to differences in host immune responses to the three strains. SAT2 elicited much more rapid and effective innate and adaptive immune responses than SAT1 and SAT3. Differences in viral production among individual hosts were thus mediated by variation in viral interactions with the host's immune responses: fast, effective adaptive immune responses limited cumulative viral production within a given host. Rapid activation of adaptive immune responses also curtailed each host's infectious period; thus, the host's antibody responses shut down viral production and the potential for transmission to other hosts. Taken together, these findings suggest that different viral life histories – characterized by variation in latency period, and time to maximum population size within the host relative to contact days – can result in similar viral fitness in terms of the amount of virus produced in an individual host. Indeed, adaptive immune activation rate and cumulative viral production were so tightly correlated [$\varrho = -0.93$]

as to be practically synonymous, indicating that viral fitness as measured by cumulative production in an individual host near exclusively reflected how speedily the host was able to mount a neutralizing antibody response to infection. At least within the parameter space defined by the viral strains and buffalo that we worked with, no other parameters of the virus-host interaction played a significant role in determining the viral production of each host.

On the other hand, acute transmission rates, the per day expected number of successfully infected contacts of the three strains, estimated in previous work [19], appear to follow variation in median viral replication rate per serotype, and not viral population size. SAT1 had the most rapid time to peak load and transmission rate, SAT2's were intermediate, and SAT3's were the lowest; whereas patterns of viral load did not match up to transmission rate variation among strains. These observations are based on a sample size of three strains: unlike our other trait associations, which evaluated variation in viral and immune dynamics across 11 hosts, our estimates of viral transmission rate are group averages. This difference arises because we cannot distinguish which individual hosts transmitted infection during our experiments - we merely recorded the timing of new infections in each group. Whole genome sequencing of virus recovered from each buffalo during the experiments might allow us to pinpoint who infected whom, elevating the precision of our transmission rate estimates to the individual level. However, even for a rapidly evolving RNA virus such as FMDV, genomic differentiation of experimental strains during a single cycle of transmission from needle-infected to in-contact hosts may not prove sufficient to identify donor and recipient hosts with confidence. As such, a greater number of viral strains would ideally need to be studied to assess the generality of these findings. Two additional observations are consistent with the finding that viral transmissibility appears to be related to within-host replication rate. We found that infection start time, latency period, and time to maximum viral load were all negatively correlated to viral growth rate. Variation in pathogen contagiousness is often related to differences in the infectious dose that is sufficient to cause infection in a new host [26] – indeed, FMDVs are notoriously able to transmit with tiny amounts of inoculum. Just a few virions suffice to propagate infections of some FMDVs to susceptible hosts [27, 28] contributing to these pathogens' hallmark contagiousness. Similarly, short incubation periods can contribute to the rapid spread of highly transmissible pathogens [26, 29–31]. As such, these observations lend credence to the idea that aggressive within-host replication in FMDVs may be indicative of high transmission capacity among hosts. It is important to note that our findings linking viral growth rate and transmission rate refer specifically to transmission during acute infection. In addition, FMDVs can transmit from carrier buffalo that retain virus in follicular dendritic cells of the palatine tonsils [32] long after the virus has been cleared from the blood. For the FMDV strains we studied, we previously estimated that SAT1 and SAT3 transmit from carrier hosts at much reduced (approx. two orders of magnitude lower) rates compared to transmission from acutely infected hosts, and carrier transmission of SAT2 is even rarer, if it occurs at all [19]. Nonetheless, at least for SAT1 and SAT3, viral transmission from carrier hosts may play a crucial role in maintaining long-term persistence of these viruses in buffalo populations, by sparking epidemics in newly susceptible calf cohorts. As such, future work should extend examination of linkages between within- and among-host dynamics of FMDVs to viral growth, maintenance and transmission in carrier hosts.

Bringing together two key findings – that adaptive immune activation drives the duration of the infectious period in each host, and viral growth rate may determine the acute viral transmission rate among hosts – we estimated $\mathcal{R}_0$, the virus' basic reproductive number from within-host dynamic parameters. We showed that estimates based on viral replication rate and adaptive activation rate qualitatively matched $\mathcal{R}_0$ estimates previously derived from observed transmission events among experimentally infected and naive buffalo [19], suggesting that viral invasion potential may be predictable from within-host dynamics. With just three viral strains and 11 host individuals to work with, these findings are necessarily tentative. We assumed linear relationships linking viral replication and transmission rates, and adaptive activation rate with infectious period, when in fact these functions may follow more complex shapes; and our power to evaluate how well $\mathcal{R}_0$ estimated from within vs among host processes match, is limited. Nonetheless, the possibility of predicting pathogen behavior in host populations from within-host experiments is tantalizing: studying pathogen strains in individual animals is far more tractable than investigating their behavior at the population scale; yet predicting which pathogen strains are likely to spread and persist in host populations of interest is an urgent priority in the face of globally accelerating pathogen emergence. Our study illustrates the value of taking a functional approach to understanding the consequences of viral diversity. By documenting variation among viral strains in terms of their life history traits, rather than focusing on genomic variation, we were able to bridge biological scales from kinetics within individual animals to transmission among hosts. This was effectively an information reduction step - zooming out to extract relevant life history signal from a sea of genomic noise to understand viral dynamics across scales. Future work could explore whether a functional approach to viral dynamics can be extrapolated down, leveraging in vitro studies of viral kinetics to predict viral life history traits and interactions with the host; and should test the generality of our findings by expanding the number viral strains that are included. This would also allow parameterization of multi-scale models that link within-host and between-host dynamics explicitly, and model validation through evaluating viral dynamics and population structure in natural host populations.

4 Summary of materials and methods

For each strain, four buffalo were needle infected and allowed to contact four naive buffalo. These naive buffalo were then captured on contact days 0, 2, 4, 6, 9, and 12 during the acute phase and again at 28 days post infection for measurement of viral and immune parameters [see [19, 23]]. The impact of route of infection on model parameters is discussed extensively in the supplementary information. We find that there were significant differences between needle and contact infected hosts, and focus our analysis here on the contact infected hosts (ie. animals infected via a natural route of infection).

4.1 Model Fitting

In this section we denote pathogen data for host j as $X_P^{(j)}$ and the data for host j collectively as $\mathbf{X}_j$. Parameter estimates were obtained by taking a weighted sum of the numerical solutions to the model model compartments as objective function. All program files and data generated by the fitting process are available on GitHub and are archived together in citeable format in the Zenodo repository (done upon submission). Data was collected for *contact infected hosts* on contact days $t = \{0, 2, 4, 6, 9, 12, 28\}$ and for *needle infected hosts* on contact days $t = \{-2, 0, 2, 4, 6, 9, 12, 28\}$. For our data fitting we first randomly draw an infection start time, $\tau_0 \in (0, t^* - 1)$ according to the posterior distributions obtained for each host in [25], where t^* is the time of the first measured positive viral load in contact days. Once done obtain initial estimates for *initial viral load*, P_0, and *viral growth rate*, r, given τ_0 and assuming a simple exponential growth model up to time t^*, that is for host i:

$$P(\tau) = P_0 e^{\tilde{r}\tau} \qquad \tau_0^{(j)} \leq \tau \leq \tau_i^*, \tag{2}$$

where $\tilde{r}$ is the net viral growth rate (in presence of innate immune response). There are two implicit biological assumptions inherent to this fitting. First, that since the innate immune response is always present estimating r is this way will account for killing of the pathogen by the innate response (thus providing a lower bound for r), and second that prior to the presence of sufficient adaptive immune response pathogen growth will be exponential (instead of logistic). The second is a common assumption in the literature when estimating viral growth rates [33, 34]. This estimate of P_0 was retained and fixed, while this estimate for viral growth rate was used as a lower bound and initial estimate for viral growth rate when simultaneously fit with other model parameters when we consider the following viral-immunological model (obtained by setting $\theta, a = 0$):

$$\begin{cases} \dfrac{dI}{d\tau} = \Lambda + \dfrac{kP(\tau)}{\gamma + P(\tau)} I(\tau) - dI(\tau) \\ \dfrac{dP}{d\tau} = \left[r\left(1 - \dfrac{P(\tau)}{K}\right) - \delta A(\tau) \right] P(\tau), \\ \dfrac{dA}{d\tau} = bA(\tau)P(\tau), \end{cases} \tag{3}$$

This simplification is numerically justified in that when fit these quantities were approximately $\mathcal{O}(10^{-10})$ (see program files on GitHub).

4.2 Practical Identifiability Analysis and Uncertainty Quantification

In order to assess identifiability, confidence in our fitting procedure, and differences in both mean *across and within serotype*, we conducted uncertainty analysis via Monte Carlo simulations. This analysis was carried out in the following manner (see [35] for detailed review of identifiability analysis for non-linear ODE models). Under the assumption that the measurement error is independently and normally distributed with variation relative in magnitude to the measured total at each data point, $X_{i,k}^{(j)}$:

$$X_{i,k}^{(j)} = g(u_{i,k}^{(j)}, \hat{\mathbf{p}} | \tau_0) + \epsilon_i^{(j)} \qquad \epsilon_i^{(j)} \sim n(0, X_{i,k}^{(j)} \cdot s^2), \tag{4}$$

where $u(\tau) = [I(\tau), P(\tau), A(\tau)]^T$, g is the true set of values at each time, and $\hat{\mathbf{p}}$ the set of true parameter values given randomly drawn τ_0, draw M start times (M = $10,000$ for each host). First, we fit the model to the original data given drawn τ_0. Next generate a new dataset according to equation (4) and refit the model. Finally for each randommly drawn infection start time calculate the average relative error between model fit parameters from the baseline data and the generated data. The results of this analysis both indicate that the key model parameters and associated quantities are all practically identifiable assuming the 40% noise level in measurement error as indicated by average relative error (ARE)

for all parameters, p_ξ, $1 \leq \xi \leq \ell$,

$$ARE_\xi = \left[\frac{100}{M} \sum_{j=1}^{M} \frac{\left| [p_\xi - \hat{p}_\xi]_{\tau_0^j} \right|}{\hat{p}_\xi|_{\tau_0^j}} \right] \leq 40\% \tag{5}$$

(see figure 2 and Supplementary Materials).

Ackwonledgments

We thank the staff of South African Parks Veterinary Wildlife Services and State Veterinary Services at Skukuza for their help with animal capture and sample collection. Lab work and field work was completed by H. Combrink, C. Coon, C. Couch, E. Devereux, B. Dugovich, K. Forssman, J. Masseloux, A. Sage, D. Sisson, H. Tavalire, and D. Trovillion. Ethical clearance was obtained from Oregon State University (ACUP 4478), South African National Parks (project no. OLAE 1157), the South African Department of Agriculture, Forestry and Fisheries: Directorate of Animal Health (Section 20 permit 12/11/1/8/3), and Onderstepoort Veterinary Research Animal Ethics Committee (100261Y5). **Funding:** J.C.M. and H.G. are supported by a U.S. NSF RAPID grant (no. DMS-2028728) and NSF grant (no. DMS-1951759), J.C.M by a Zuckerman Postdoctoral Scholarship and H.G. by a grant from the Simons Foundation/SFARI 638193. Experimental work and Epidemic scale model development was supported by USDA-NIFA AFRI grant 2013-67015-21291 and by the UK Biotechnology and Biological Sciences Research Council grant BB/L011085/1 as part of the joint USDA-NSF-NIH-BBSRC Ecology and Evolution of Infectious Diseases program. S.G. was supported by UK Biotechnology and Biological Sciences Research Council grants BBS/E/I/00007030, BBS/E/I/00007036, and BBS/E/I/00007037. Ongoing work is supported by the joint NSF-NIH-NIFA Ecology and Evolution of Infectious Disease (number 2208087)

References

[1] Raina K Plowright, Susanne H Sokolow, Michael E Gorman, Peter Daszak, and Janet E Foley. Causal inference in disease ecology: investigating ecological drivers of disease emergence. *Frontiers in Ecology and the Environment*, 6(8):420–429, 2008.

[2] Montira J Pongsiri, Joe Roman, Vanessa O Ezenwa, Tony L Goldberg, Hillel S Koren, Stephen C Newbold, Richard S Ostfeld, Subhrendu K Pattanayak, and Daniel J Salkeld. Biodiversity loss affects global disease ecology. *Bioscience*, 59(11):945–954, 2009.

[3] Nina Wale and Meghan A Duffy. The use and underuse of model systems in infectious disease ecology and evolutionary biology. *The American Naturalist*, 198(1):69–92, 2021.

[4] Yuyi Xue and Yanni Xiao. Analysis of a multiscale hiv-1 model coupling within-host viral dynamics and between-host transmission dynamics. *Mathematical Biosciences and Engineering*, 17(6):6720–6736, 2020.

[5] Rocio Caja Rivera, Shakir Bilal, and Edwin Michael. The relation between host competence and vector-feeding preference in a multi-host model: Chagas and cutaneous leishmaniasis. *Mathematical Biosciences and Engineering*, 17(5):5561–5583, 2020.

[6] Junbo Jia, Wei Shi, Pan Yang, and Xinchu Fu. Immunization strategies in directed networks. *Mathematical Biosciences and Engineering*, 17(4):3925–3952, 2020.

[7] Sarah Kadelka and Stanca M Ciupe. Mathematical investigation of hbeag seroclearance. *Mathematical Biosciences and Engineering*, 16(6), 2019.

[8] Cameron J Browne and Chang-Yuan Cheng. Age-structured viral dynamics in a host with multiple compartments. *Mathematical Biosciences and Engineering*, 17(1), 2020.

[9] Ephraim O Agyingi, Tamas I Wiandt, Laurence U Buxbaum, and Bolaji N Thomas. Modeling the immune system response: an application to leishmaniasis. *Mathematical Biosciences and Engineering*, 17(2):1253–1271, 2020.

[10] Winston Garira. The research and development process for multiscale models of infectious disease systems. *PLoS computational biology*, 16(4):e1007734, 2020.

[11] Ashlee N Ford Versypt. Multiscale modeling in disease. *Current Opinion in Systems Biology*, 2021.

[12] Rebecca B Garabed, Anna Jolles, Winston Garira, Cristina Lanzas, Juan Gutierrez, and Grzegorz Rempala. Multi-scale dynamics of infectious diseases, 2020.

[13] Odo Diekmann, Johan Andre Peter Heesterbeek, and Johan AJ Metz. On the definition and the computation of the basic reproduction ratio r 0 in models for infectious diseases in heterogeneous populations. *Journal of mathematical biology*, 28(4):365–382, 1990.

[14] J. A. W. Coetzer, G. R. Thomson, and R. C. Tustin. *Infectious Diseases of Livestock: With Special Reference to Southern Africa*. Oxford University Press, Oxford, 1994.

[15] MD Gainaru, Jan J Esterhuysen, W Bruce, Attilio Pini, Roy G Bengis, and GR Thomson. Foot-and-mouth disease and the african buffalo (syncerus caffer).: Ii. virus excretion and transmission during acute infection. 1986.

[16] GR Thomson, W Vosloo, JJ Esterhuysen, and RG Bengis. Maintenance of foot and mouth disease viruses in buffalo (syncerus caffer sparrman, 1779) in southern africa. *Revue scientifique et technique (International Office of Epizootics)*, 11(4):1097–1107, 1992.

[17] Francois Maree, Lin-Mari de Klerk-Lorist, Simon Gubbins, Fuquan Zhang, Julian Seago, Eva Pérez-Martín, Liz Reid, Katherine Scott, Louis van Schalkwyk, Roy Bengis, et al. Differential persistence of foot-and-mouth disease virus in african buffalo is related to virus virulence. *Journal of virology*, 90(10):5132–5140, 2016.

[18] W Vosloo, AD Bastos, E Kirkbride, JJ Esterhuysen, D Janse Van Rensburg, RG Bengis, DW Keet, and GR Thomson. Persistent infection of african buffalo (syncerus caffer) with sat-type foot-and-mouth disease viruses: rate of fixation of mutations, antigenic change and interspecies transmission. *Journal of General Virology*, 77(7):1457–1467, 1996.

[19] Anna Jolles, Erin Gorsich, Simon Gubbins, Brianna Beechler, Peter Buss, Nick Juleff, Lin-Mari de Klerk-Lorist, Francois Maree, Eva Perez-Martin, O.L. van Schalkwyk, Katherine Scott, Fuquan Zhang, Jan Medlock, and Bryan Charleston. Endemic persistence of a highly contagious pathogen: Foot-and-mouth disease in its wildlife host. *Science*, 374(6563):104–109, 2021.

[20] Caroline K. Glidden, Brianna Beechler, Peter Erik Buss, Bryan Charleston, Lin-Mari de Klerk-Lorist, Francois Frederick Maree, Timothy Muller, Eva Pérez-Martin, Katherine Anne Scott, Ockert Louis van Schalkwyk, and Anna Jolles. Detection of pathogen exposure in african buffalo using non-specific markers of inflammation. *Frontiers in Immunology*, 8:1944, 2018.

[21] Carolina Stenfeldt, Peter MH Heegaard, Anders Stockmarr, Kirsten Tjørnehøj, and Graham J Belsham. Analysis of the acute phase responses of serum amyloid a, haptoglobin and type 1 interferon in cattle experimentally infected with foot-and-mouth disease virus serotype o. *Veterinary research*, 42(1):1–10, 2011.

[22] Claire E Couch, Morgan A Movius, Anna E Jolles, M Elena Gorman, Johanna D Rigas, and Brianna R Beechler. Serum biochemistry panels in african buffalo: Defining reference intervals and assessing variability across season, age and sex. *PLoS One*, 12(5):e0176830, 2017.

[23] Eva Perez-Martin, Brianna Beechler, Katherine Scott, Lin-Mari de Klerk-Lorist, Fuquan Zhang, Georgina Limon, Brian Dugovich, Simon Gubbins, Arista Botha, Nicholas Juleff, Robyn Hetem, Louis van Schalkwyk, Francois F. Maree, Anna Jolles, and Bryan Charleston. Viral dynamics and immune responses to foot-and-mouth disease virus in african buffalo (syncerus caffer). *bioRxiv*, 2021.

[24] Ian R Tizard. *Veterinary Immunology-E-Book*. Elsevier Health Sciences, 2017.

[25] Simon Gubbins. SimonGubbins/FMDVInBuffalo: Release for publication 1.0.0, July 2021.

[26] Paul E. M. Fine. The Interval between Successive Cases of an Infectious Disease. *American Journal of Epidemiology*, 158(11):1039–1047, 12 2003.

[27] M. Quan, C.M. Murphy, Z. Zhang, and S. Alexandersen. Determinants of early foot-and-mouth disease virus dynamics in pigs. *Journal of Comparative Pathology*, 131(4):294–307, 2004.

[28] S. Alexandersen, M. Quan, C. Murphy, J. Knight, and Z. Zhang. Studies of quantitative parameters of virus excretion and transmission in pigs and cattle experimentally infected with foot-and-mouth disease virus. *Journal of Comparative Pathology*, 129(4):268–282, 2003.

[29] Hiroshi Nishiura, Natalie M. Linton, and Andrei R. Akhmetzhanov. Serial interval of novel coronavirus (covid-19) infections. *International Journal of Infectious Diseases*, 93:284–286, 2020.

[30] Nicholas C Grassly and Christophe Fraser. Mathematical models of infectious disease transmission. *Nature Reviews Microbiology*, 6(6):477–487, 2008.

[31] Philip E Sartwell. The distribution of incubation periods of infectious disease. *American journal of epidemiology*, 141(5):386–394, 1995.

[32] Nicholas Juleff, Miriam Windsor, Elizabeth Reid, Julian Seago, Zhidong Zhang, Paul Monaghan, Ivan W Morrison, and Bryan Charleston. Foot-and-mouth disease virus persists in the light zone of germinal centres. *PloS one*, 3(10):e3434, 2008.

[33] Kasia A. Pawelek, Giao T. Huynh, Michelle Quinlivan, Ann Cullinane, Libin Rong, and Alan S. Perelson. Modeling within-host dynamics of influenza virus infection including immune responses. *PLOS Computational Biology*, 8(6):1–13, 06 2012.

[34] A. L. Lloyd. The dependence of viral parameter estimates on the assumed viral life cycle: limitations of studies of viral load data. *Proceedings of the Royal Society of London. Series B: Biological Sciences*, 268(1469):847–854, 2001.

[35] Hongyu Miao, Xiaohua Xia, Alan S. Perelson, and Hulin Wu. On identifiability of nonlinear ode models and applications in viral dynamics. *SIAM Reviews*, 53(1):3–39, 2011.